Available online at www.sciencedirect.com
SCIENCE DIRECT
Journal of Molecular Graphics and Modelling 23 (2005) 490–502
Journal of Molecular Graphics and Modelling
www.elsevier.com/locate/JMGM

A model for the interaction between plant GAPN and 14-3-3ζ using protein–protein docking calculations, electrostatic potentials and kinetics

Diego M. Bustos [a], Alberto A. Iglesias [b,*]

[a] *Instituto Tecnológico de Chascomús (IIB-INTECH), Camino Circunv, Laguna km 6, CC 164, B7130IWA Chascomús, Argentina*
[b] *Laboratorio de Enzimología Molecular, Bioquímica Básica de Macromoléculas, Facultad de Bioquímica y Ciencias Biológicas, UNL, Paraje "El Pozo", CC 242, S3000ZAA Santa Fe, Argentina*

Received 17 June 2004; received in revised form 25 March 2005; accepted 29 March 2005
Available online 17 May 2005

Abstract

Phosphorylated non-phosphorylating glyceraldehyde-3-phosphate dehydrogenase (EC 1.2.1.9; GAPN) found in heterotrophic cells of wheat is activated by $MgCl_2$. The divalent cation disrupts the interaction between GAPN and a 14-3-3 regulatory protein. This effect is quite remarkable, since it has previously been shown that 14-3-3 binding to a target protein requires divalent cations as Mg^{2+} or Ca^{2+}. Binding of the divalent cation to 14-3-3 causes an increase in surface hydrophobicity. Crystal structure of a 14-3-3-target protein complex has been only determined for serotinin *N*-acetyltransferase. We utilized a model of a subunit of plant GAPN and the crystallographic structure of human 14-3-3ζ to shape the complex between theses two proteins. Initial dockings were performed with the BiGGER program, which allows an exhaustive search of translational and rotational space. A filtering procedure was then applied to reduce the number of complexes to a manageable number. We predict the structural characteristics of GAPN–14-3-3ζ binding process, proposing that the main attractive force in this complex derives from electrostatic interactions. The predicted model was corroborated by analysis of kinetic behavior of GAPN and its relationship with pH and ionic strength conditions. This study provides a variant on the interaction of 14-3-3 with target proteins, thus affording a wider scenario to establish possible structural models for this remarkable family of regulatory proteins.

Keywords: Glyceraldehyde-3-phosphate; Non-phosphorylating; GAPN; 14-3-3 Proteins; Protein–protein docking

1. Introduction

Non-phosphorylating glyceraldehyde-3-phosphate dehydrogenase (EC 1.2.1.9; GAPN) has been identified as a member of the aldehyde dehydrogenase superfamily [1]. The enzyme catalyzes the irreversible, $NADP^+$-dependent, oxidation of glyceraldehyde-3-phosphate (Ga3P) into 3-phosphoglycerate (3-PGA) [2,3]. GAPN has been found in green algae, higher plants [1,4], and some specialized bacteria [1,5]. In photosynthetic cells the enzyme is involved in a shuttle system exporting photogenerated NADPH from the chloroplast, and thus it plays a key role in the supply of reducing power to the cytosol [3]. In plants, GAPN is also found in non-photosynthetic tissues, such as endosperm, shoots, cotyledons, and roots [4,6,7]. The function played by this enzyme in heterotrophic plant cells is less clear. It has been proposed that in non-green cells GAPN could couple NADPH production needed for anabolic reactions to glycolysis [1].

GAPN activity is carried out by a catalytic domain in the enzyme whose structure and specific amino acid residues are highly or absolutely conserved in the aldehyde dehydrogenase superfamily [1]. This characteristic structure has been found to involve three subdomains with highly conserved sequences [7]. Crystallographic structures and kinetic studies of GAPN from the bacterium *Streptococcus mutans* (GAPN*sm*) have enabled the determination of the enzyme catalytic mechanism [8]. It starts with the binding of

* Corresponding author. Tel.: +54 342457 5216x217; fax: +54 342457 5221.
E-mail address: iglesias@fbcb.unl.edu.ar (A.A. Iglesias).

1093-3263/$ – see front matter © 2005 Elsevier Inc. All rights reserved.
doi:10.1016/j.jmgm.2005.03.002

$NADP^+$ to apo-GAPN, which induces a local conformational change of the active site [8], with at least a reorientation of side chains of amino acids Cys^{302} and Glu^{268}. Four other residues found conserved in the GAPN family (Arg^{124}, Tyr^{170}, Arg^{301}, and Arg^{459}) seem to be involved in the recognition of the other substrate, D-Ga3P, as well as in catalysis [2,3].

GAPN from wheat endosperm and shoots requires Mg^{2+} to achieve maximal activity [9]. The latter could be associated with recent findings from our laboratory on the phosphorylation of GAPN from plant heterotrophic tissues [7] and its interaction with 14-3-3 regulatory proteins [9]. Data derived from size exclusion chromatography and co-immunoprecipitation demonstrated that Mg^{2+} exerts the disruption of a protein–protein interaction between native, phosphorylated GAPN and a 14-3-3 protein [9]. These novel findings showing that GAPN activity is under control by post-translational modification, dark-to-light variation of Mg^{2+} concentration [10], and interaction with regulatory proteins, open a new scenario on the way of how carbohydrates can be utilized to produce ATP or NADPH in the cytosol of non-green cells from plants [7,9,11].

One hallmark of signal transduction events is the phosphorylation-induced transition of a protein from one active state to another [12]. However, it is becoming clear that, in many cases, phosphorylation by itself is not sufficient to induce changes in activity. Rather, it is the phosphorylation-induced association with 14-3-3 proteins that results in the transition to changes in activity [12]. In plants, 14-3-3 proteins were found to regulate the activity of enzymes involved in primary carbon metabolism, nitrogen assimilation and generation of protons gradient [13].

Crystal structures of both τ and ζ isoforms of 14-3-3 show that they are highly helical, dimeric proteins [14,15]. Each monomer is composed of nine anti-parallel α-helices, organized into an N-terminal and a C-terminal domain. The dimer forms a large, negatively charged channel [16]. The 14-3-3 proteins bind to targets containing the consensus sequence RXXpS/pTXP (named mode 1) or RXXXpS/pTXP (mode 2), with the coordination of pSer by three absolutely conserved amino acid residues, Lys^{49}, Arg^{56} and Arg^{127}, as originally described [17,18]. However, phosphorylation of the target protein is not the only factor controlling the binding of 14-3-3. Although hydrophobic interactions could be a main force determining 14-3-3-target interactions [19], electrostatic attraction has long been recognized as a key driving force for fast protein–protein associations [20].

The interaction of 14-3-3s with their targets specifically requires millimolar concentrations of a divalent cation [21] such as Mg^{2+}, Ca^{2+} or Mn^{2+}. The structural model shows that binding of the divalent cation to the 14-3-3 causes an increase in surface hydrophobicity, as was monitored using the fluorescent probe bis-ANS [4,4′-bis(1-anilinonapthalene 8-sulfonate) [19]. Interestingly, the interaction of plant phosphorylated GAPN with 14-3-3 was found to be released by Mg^{2+}, thus constituting a distinctive example respect to the way by which the regulatory protein binds to a target enzyme [9]. The prediction of a structural model for the complex formed between GAPN and 14-3-3 is thus particularly important to understand the odd behaviour of the divalent cation in this protein–protein interaction.

The 14-3-3-affinity purification of more than 200 human phosphoproteins [22] reveals that 14-3-3 interacts with several cellular proteins to regulate metabolism, proliferation and trafficking. From this, it is clear that even when automated crystallography techniques were utilized, the elucidation of the fine structure of all the complexes between 14-3-3 and target proteins is far from being available. Under this scenario, the developing of new in silico structural approaches become practically relevant. Docking algorithms are currently being developed for the correct analysis of protein–ligand complexes. However, to predict protein–protein interactions is more difficult, requiring of other data to select for the best model. In the present work, we utilized an in silico structural approach to study the plant phosphorylated GAPN–14-3-3ζ complex using protein docking calculations, biochemical data filtering and kinetic and hysteretic behaviour experiments. The derived model is compared with those previously developed, to understand the distinctive effect of the divalent cation in the interaction between GAPN and 14-3-3.

2. Material and methods

2.1. Multiple sequence alignment

The sequences of GAPN monomers were aligned using the DIALIGN multiple sequence alignment algorithm [23], that includes the following steps: (1) pairwise alignment using Needleman and Wunsch algorithm modified to use zero end gap penalties; (2) evolutionary tree construction with a ‘‘neighbour-joining algorithm’’, to determine the order of alignment and to calculate relative weight of sequences and profiles from the branch lengths; and (3) traverse the tree from top to bottom, aligning the closest sequences or profiles. A multi-protein sequence alignment of GAPN monomers was generated automatically by the DIALIGN [23] method and then it was manually adjusted around residues 240–255 (in plant GAPN), in order to correctly align the motif GxxxG/A between prokaryotic and plant GAPNs.

2.2. Plant GAPN and its interaction with 14-3-3: sequences and 3D model building

Three-dimensional models (GAPNpls) of five known plant GAPNs were constructed using crystal structure coordinates of GAPN*sm* (PDB code: 1EUH) as template and Modeller v6.0 program [24]. Sequences of plant GAPNs were obtained from the Genebank. Modeller program is completely automated and capable of generating energy

minimized protein models by satisfying restraints on bond distances and dihedral angles. The identity percentage between models and template sequences is 52%, which is in good agreement with Modeller requirements. GAPNpls were based in the protein at the unphosphorylated state, and its evaluation was conducted using the WHATIF program [25].

Protein coordinates for human 14-3-3ζ were obtained from the Protein Databank (PDB code 1A4O, subunit A and B). In this structure, monomeric 14-3-3 contains nine anti-parallel α-helices arranged into an N-terminal and a C-terminal domain. Although it has been pointed out the existence of a tenth α-helix in plant 14-3-3 (unsolved in the human isoform, see reference [26]), it would localize far away from the target binding site, and consequently playing no relevant role in the proposed model.

All GAPN residues within 8 Å of the putative 14-3-3 binding site (^{401}RINSVEE) differing from the GAPN template residue were energy-minimized by AMBER force field [27], implemented on HyperChem 5.0, according to the following procedure. Coordinates of the backbone atoms in plant GAPN were set to the values of the corresponding atoms in GAPN*sm*. Similarly, coordinates of side chain atoms of the conserved residues were set to the values of the corresponding coordinates of GAPN*sm* atoms as well. In contrast, side chains of no conserved residues were set in an extended conformation. The resulting structure of plant GAPN was energy minimized in vacuo using a distance-dependent dielectric constant, and equal electrostatic and van der Waals forces. Minimization was carried out in one step, where the residues were completely relaxed. The resulting structure exhibited a root mean square deviation (rmsd) minor to 1.6 Å from the starting X-ray structure when all the backbone atoms were compared, which represents a reasonable value.

2.3. Protein docking

Molecular interaction simulations were performed using the docking program BiGGER [28]. Although this program only succeeded in modelling one of the five critical assessment of prediction of interactions (CAPRI) targets, these results seem to be more due to the difficulty of the task than to shortcomings in the method, and BiGGER could suggest useful models in a setting where some experimental data were available, which is our case. This algorithm performs a complete and systematic search in the binding space of both molecules. The surface of each partner is represented as a binary (0, 1) grid at 1 Å resolution, and surface contact is estimated by counting the superposition of surface cells (those marked with 1 in each grid). The core region of each partner is represented as another binary matrix, and superposition of these core regions indicates excessive overlap and is forbidden. A population of 1000 candidate protein–protein-docked geometries is generated and selected, based on the geometric complementarities and amino acid pairwise affinities between the two molecular surfaces. In this process, the algorithm enables implicit treatment of molecular flexibility.

A candidate model is rejected if it does not have a higher surface contact score than the lowest ranking of the models retained at that point. If it has a higher score, it replaces the lowest ranking model if it passes the second filter, which is a neural network that evaluates the amino acid contacts between the partners. This network was trained with a large number of examples to distinguish between correct and incorrect complexes. In a subsequent step, putative docked structures are ranked using an interaction scoring function, which combines several interaction terms thought to be relevant for the stabilization of protein complexes. The latter includes: geometric packing of the surfaces, explicit electrostatic interactions, desolvation energy, and pairwise propensities of the amino acid side chains to contact across the molecular interface. In the ab initio simulations, the entire molecular surface was searched using absolutely no additional information regarding the binding sites. After this first step, a biochemical filter was utilized in order to reduce the quantity of complexes to a manageable number. Specifically, the amino acid residues Ser^{404} from GAPN and Lys^{49}, Arg^{56} and Arg^{127} from 14-3-3 protein were selected and distances between these moieties sorted all complexes.

The peptide ARAApSAPA (designed by Carol MacKintosh, University of Dundee, UK) was docked using GRAMM v1.03 program [29] that may be used for a protein and for a smaller compound as well. We performed this docking because the peptide was previously shown to interact with 14-3-3 competitively with GAPN [9] and thus it afford useful information on the region in 14-3-3 where the interaction with plant GAPN takes place. The following parameters were utilized: atching mode (generic/helix) = -generic; grid step = 1.7; repulsion (attraction is always −1) = 5.; attraction double range (fraction of single range) = 0.; potential range type (atom_radius, grid_step) = atom_radius; projection (blackwhite, grey) = blackwhite; representation (all, hydrophobic) = all; number of matches to output = 1000; angle for rotations, (10°, 12°, 15°, 18°, 20°, 30°, 0°—no rot.) = 10.

2.4. Electrostatic potentials

Electrostatic potentials were obtained from Swiss pdb viewer v3.7 program. The solvent was described in terms of a bulk dielectric constants (=80), whereas GAPN and 14-3-3 were described in terms of the coordinates of individual atoms as well as atomic partial charges and dielectric constant (protein) = 4.0. Computational methods were Poisson–Boltzmann equations; and solvent ionic strength = 0.0 mol/l. Coordinates for the experimentally determined 14-3-3ζ without any divalent cation and modelled GAPN structure were used in the calculations.

No difference was observed between the structures of the peptide bound and peptide free states of 14-3-3 [30],

suggesting that no conformational change is induced by binding of the ligand to 14-3-3. Indeed, these crystallographic structures were obtained at different concentrations of Mg^{2+}, so it is possible that no conformational change occurs in the presence of this cation as well. Although an increase of surface hydrophobicity was monitored in 14-3-3 [19] in the presence of divalent cations, no experimental evidence of conformational change has been reported at the present time.

2.5. Kinetic studies

Initial velocity studies were performed by following NADPH formation at 340 nm in a Spectronic 20 spectrophotometer, essentially as previously described [7,9]. Concentrations of $NADP^+$ and D-Ga3P were fixed at 0.11 and 1.2 mM, respectively. Studies on the hysteretic behaviour were performed as before [31]. Samples partially purified from wheat endosperm and containing the GAPN–14-3-3 complex [7,9] were incubated at 30 °C, the temperature used for activity assays, in a medium containing 50 mM Tricine–NaOH (pH 8.5), 1 mM 2-mercaptoethanol, and NaCl at the specified concentrations. After 5 min preincubation with the different concentrations of NaCl, an aliquot was withdrawn and immediately assayed for activity in media containing 10 mM $MgCl_2$. The time course of the reaction was continuously registered and the non-linear (lag exhibiting) transient analyzed. The kinetic transient followed a first order exponential increase, with data fitting the equation described by Neet and Ainslie [32]:

$$[P] = V_{ss}t - \left[\frac{(V_{ss} - V_i)}{k_{obs}}\right][1 - \exp(-k_{obs}t)]$$

where V_i and V_{ss} are the initial and the steady state (linear) velocities, respectively; t is time of reaction and k_{obs} is the apparent rate constant for the transition between V_i and V_{ss}. For a more compressive analysis k_{obs} was transformed into $k_{obs}^{-1} = \tau$. The experimental data obtained under linear reaction conditions (V_{ss}) were fitted to the generalized Hill equation by a non-linear least square regression kinetics computer program [33]. This program was used to determine sigmoidicity in the respective substrate saturation curve, by calculating Hill coefficients (n_H). Since n_H was not significantly different from 1 in all cases, the same computer program was utilized to fit data to the Michaelis Menten equation. One unit (U) is defined as the amount of enzyme that catalyzes the formation of 1 μmol NADPH/min under the specified assay conditions.

3. Results and discussion

3.1. Homology modelling of GAPN

A crystal structure (1.8 Å resolution) corresponding to a monomer of apo-GAPN from *S. mutans* (GAPN*sm*; PDB code 1EUH) was utilized as template to build a homology model of five known plant GAPN homotetrameric enzymes. Prokaryotic and eukaryotic protein sequences have 52% identities, being thus in good agreement to perform homology modelling procedure. The multi-protein sequence alignment of GAPN, automatically generated by the DIALIGN [23] method and manually adjusted between prokaryotic and plant GAPNs, exhibited sequence blocks of interest as shown in Fig. 1. In addition, even when good homology exists between plant and GAPN*sm* subunits the overall model was further refined (see Section 2 for details).

The overall topology of the GAPN models was similar to X-ray structure of GAPN*sm* [8]. Each monomer can be divided into three domains (Fig. 2): (i) a cofactor binding domain composed of a core which resembles the Rossmann fold (residues 145–252) flanked by five helices and four strands (residues 2–118, 450–464), (ii) a catalytic α/β domain (residues 253–449), and (iii) a small protruding domain (residues 119–144 and 465–475) enabling oligomerization.

The most remarkable feature in our models is that two Cys residues (Cys^{271} and Cys^{422} in *Triticum aestivum*) strictly conserved in the sequence of plant GAPNs, but absent in the enzyme from prokaryotes (Fig. 1), are separated 2.2 Å and in the right orientation to form a disulfide bond [25] (Fig. 2). To the best of our knowledge, the existence of this disulfide bond has never been described and its relevance for the GAPN stability during oxidative stress in plants is under experimentation (unpublished result from our laboratory).

Quality of the model was assessed by using different validation tools. We performed proline puckering, packing quality, and stereochemistry of main-chain and side-chain residues using program WHATIF [25]. The rmsd between template and models using all main-chain atoms was found to be minor to 1.6 Å. Fig. 2 shows a superposition of C-A backbones between plant and *S. mutants* GAPNs. Ramachandran plot statistics indicated that 92 ∼ 96.5% of the main-chain dihedral angles (Φ and Ψ) are found in the most favourable region. The resulting Ramachandran *Z*-score = −2.511, expresses how well the backbone conformations of all residues are corresponding to the known allowed areas in the Ramachandran plot, being the value within expected ranges for well-refined structures [25].

3.2. GAPN domains interacting with 14-3-3 proteins

We have previously analyzed [7,9] possible phosphorylation sites in plant GAPN, which could be relevant in the interaction of the enzyme with 14-3-3 proteins. In such an analysis, Ser^{404} in the enzyme from *T. aestivum* exhibits the highest phosphorylation probability, being the only site exposed to solvent (and accessible to a putative kinase) into GAPN homotetramer. Indeed, the sequence around Ser^{404} (see Fig. 1) is more potentially able to bind a 14-3-3 protein. Analysis of this sequence shows that it lacks a Pro residue (+2 from pSer) present in other proteins interacting with 14-

```
A.thailiana      267   GKDACIVLDD A----DLDLV ASNIIKGGFS YSGQRCTAVK VVLVMESVAD
A.graveolens     267   GKDACIVLED A----DLDLV ASNVIKGGFS YSGQRCTAIK VILVMQSVAD
O.sativa         270   GKDACVVLED A----DLDLV AANIVKGGFS YSGQKCTAVK VVLIMESVAD
P.sativum        267   GKDACIVLED A----DLDLV AANIIKGGFS YSGQRCTAVK VVLVMESVAD
N.plumbagini     267   GKDACIVLED A----DLDLA AGSIVKGGFS YSGQRCTAVK VVLVMESVAD
T.aestivum       267   GKDACIVXEX A----DLDLV XANIVKGGFS YSGQRCNAVK VVLIMEXXAD
Z.mays           269   GKDACIVLED A----DLDLV SANIVKGGFS YSGQRCTAVK VVLIMESIAD
S.mutans         253   GKDSAIVLED A----DLELT AKNIIAGAFG YSGQRCTAVK RVLVMESVAD
S.solfataric     245   GSDPIIILED A----NIERA SSIAVRARFE YAGQNCNAGK RIIVREEIYD
S.solfataric2    273   GGDPAIVLSD A----DLAWA AQRIAAGIIS YTGQRCDSVK LVLVEEEVYD
T.tenax          266   GGDPAIVLED A----DLDLA ADKIARGIYS YAGQRCDAIK LVLAERPVYG
M.jannaschii     243   GVNPNIVLKD A----DLNKA VNALIKGSFI YAGQVCISVG MILVDESIAD
S.coelicolor     252   GNGAAVVLAD wasdeDLDRA ATRIATFSNY QGGQSCISVQ RVIADAAVYD
S.pyogenes       245   GKDSAIVLED A----DLVLA AKNIVAGAFG YSGQRCTAVK RVLVMDKVAD
S.pyogenes2      253   GKDSAIVLED A----DLALA AKNIVAGAFG YSGQRCTAVK RVLVMDKVAD
S.pneumoniae     252   GKDAALVLED A----DLEHA AKQIVAGAFS YSGQRCTAIK RVIVLESVAD

A.thailiana      395   PVVPVLRINS VEEGINHCNA SNFGLQGCVF TKDINKAILI SDAMETGTVQ
A.graveolens     395   PILPVIRINS AEEGIHHCNA SNFGLQGCVF TRDINKAMLI SDAMESGTIQ
O.sativa         406   PVLPVIRINS VEEGIHHCNA SNFGLQGCVF TKDINKAIMI SDAMETGTVQ
P.sativum        395   PVLPVIRINS VEEGIHHCNA SNFGLQGCVF TKDINKAIMI SDAMESGTVQ
N.plumbagini     395   PVLPVIRINS VEEGIHHCNA SNFGLQGCVF TKDINKAILI SDAMETGTVQ
T.aestivum       395   PVLPVIRINS VEEGIHHCNA SNFGLQGCVF TRDINKAIMI SDAMESGTVQ
Z.mays           397   PVLPVIRINS VEEGIHHCNA SNFGLQGCIF TRDINKAILI SDAMETGTVQ
S.mutans         381   PVLPIIRVTS VEEAIEISNK SEYGLQASIF TNDFPRAFGI AEQLEVGTVH
S.solfataric     376   PIVPIVSVKS DEEAIRIANS TEYGLQSAIF TNDVNRALKL SRELKFGAVI
S.solfataric2    407   SAALLIKVKN IDEALEISNS RKYGLDAAIF GKDINKIRKL QRFLEVGAIY
T.tenax          399   PVASAVEVKD LDQAIELANG RPYGLDAAVF GRDVVKIRRA VRLLEVGAIY
M.jannaschii     371   PVIPIIR-TN EEEMIDIANS TEYGLHSAIF TNDINKSLKF AENLEFGGVV
S.coelicolor     385   PVLSVQRVTG EAEAFAAVND SKYGLQAGVF THDLQAAFRA HRALEVGGVV
S.pyogenes       373   PVLPIIRVTT VEEAIKISNE SEYGLQASIF TTNFPKAFGI AEQLEVGTVH
S.pyogenes2      381   PVLPIIRVTT VEEAVKISNE SEYGLQASIF TTNFPKAFGI AEQLEVGTVH
S.pneumoniae     380   PVLPIIRVAS VEEAIAFANE SEFGLQSSVF TNDFKKAFEI AEKLEVGTVH

A.thailiana      445   INSAPARGPD HFPFQGLKDS GIGSQGVTNS INLMTKVKTT VINLPTPSYS
A.graveolens     445   INSAPARGPD HFPFQGLKDS GIGSQGITNS INMMTKIKTT VINLPSPSYT
O.sativa         456   INSAPARGPD HFPFQGLKDS GIGSQGITNS INMMTKVKST VINLPSPSYT
P.sativum        445   INSAPARGPD HFPFQGIKDS GIGSQGITNS INMMTKVKTT VINLPSPSYT
N.plumbagini     445   INSAPARGPD HFPFQGIKDS GIGSQGITNS INMMTKVKTT VINLPTPSYT
T.aestivum       445   INSAPARGPD HFPFQGLKDS GIGSQGITNS INMMTKVKST VINLPSPSYT
Z.mays           447   INSAPARGPD HFSFQGLKDS GIGSQGITNS INMMTKVKST VINLPSPSYT
S.mutans         431   INNKTQRGTD NFPFLGAKKS GAGIQGVKYS IEAMTTVKSV VFDIK-----
S.solfataric     426   INDSTRLRWD SLAFGGFKKS SIGREGVRET MLEMTENKLI AITLl-----
S.solfataric2    457   INDYPRHGIG YFPFGGRKDS GIGREGIGYT IQYVTAYKSI VYNYKGKGIW
T.tenax          449   INDMPRHGIG YYPFGGRKKS GVFREGIGYA VEAVTAYKTI VFNYKGKGVW
M.jannaschii     420   INDSSLFRQD NMPFGGVKKS GLGREGVKYA MEEMSNIKTI IISk------
S.coelicolor     435   IGDIPSYRAD QMPYGGAKQS GVGREGVKFA MDDYTYERVL VLTglal---
S.pyogenes       423   LNNKTQRGTD NFPFLGAKKS GAGVQGVKYS IEAMTTVKSV VFDIQ-----
S.pyogenes2      431   LNNKTQRGTD NFPFLGAKKS GAGVQGVKYS IEAMTTVKSV VFDIQ-----
S.pneumoniae     430   INNKTQRGPD NFPFLGVKGS GAGVQGIKYS IEAMTNVKSI VFDVK-----
```

Fig. 1. C-terminal alignment of primary structure corresponding to plant and prokaryotic GAPNs. Highly conserved residues: Cys, canonical 14-3-3 binding sites, and His are in black background. Gaps in the sequences were replaced by dashes. *A. thaliana*: *Arabidopsis thaliana*. *A. graveolens*: *Apium graveolens*. *O. sativa*: *Oryza sativa*. *P. sativum*: *Pisum sativum*. *N. plumbagini*: *Nicotiana plumbaginifolia*. *T. aestivum*: *Triticum aestivum*. *Z. mays*: *Zea mays*. *S. mutans*: *Streptococcus mutans*. *S. solfataric*: *Sulfolobus solfataricus isozyme 1*. *S. solfataric2*: *Sulfolobus solfataricus isozyme 2*. *T. tenax*: *Thermoproteus tenax*. *M. jannaschii*: *Methanococcus jannaschii*. *S. coelicolor*: *Streptomyces coelicolor*. *S. pyogenes*: *Streptococcus pyogenes isozyme 1*. *S. pyogenes2*: *Streptococcus pyogenes isozyme 2*. *S. pneumoniae*: *Streptococcus pneumoniae*.

3-3 [34]. However, there are many evidences that proteins lacking this residue bind 14-3-3 proteins as well [35,36]. Indeed, sequence analysis reveals that sites lacking the Pro residue have a Val in position +1, similar to what is found in this site from plant GAPNs (Fig. 1). Several proteins bind to 14-3-3 via unconventional phosphopeptide binding sequences, like cardiac phosphofructokinase-2 (PFK-2), whose binding to 14-3-3s is dependent on phosphorylation at Ser^{483} (RNYpSVGS) by protein kinase B, which does not precisely conform to a canonical 14-3-3-binding motif [35]. Also, three different K^+-channels and the nicotinic receptor have a 14-3-3 binding motif without Pro residue and with a Val residue in +1 position [36]. The site in GAPN potentially interacting with 14-3-3 proteins is exposed to the solvent either in the monomeric or tetrameric structures of the enzyme (data not shown). Taking this into account, building of a structural model that includes the 14-3-3 binding pocket was performed from the alignment onto template monomer.

In our previous report [9], we showed that the peptide ARAApSAPA (designed by Carol MacKintosh, University

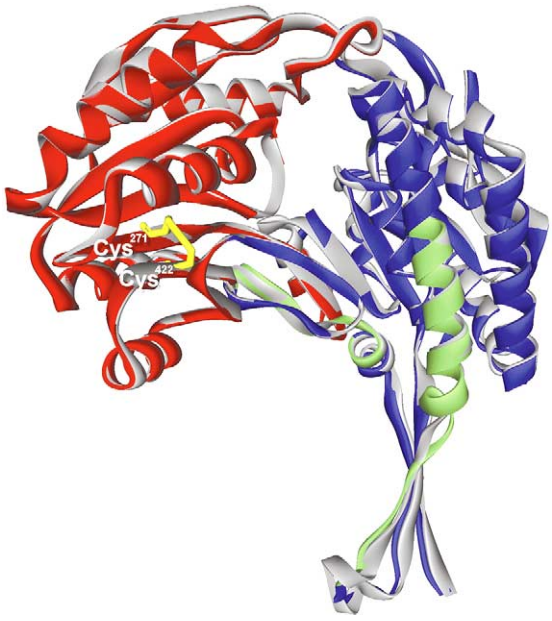

Fig. 2. Superimposition of the C-A trace of each monomer of GAPN*sm* (grey) and plant GAPNs (colours). The superimposition of the monomer structures was done with Chemera [28]. The rmsd between template and models was minor to 1.6 Å. Each monomer can be divided into three domains: a cofactor binding domain (similar to Rossmann fold) and five helices and four strands, in blue; a catalytic domain in red; and the oligomerisation domain, in green. Cys^{271} and Cys^{422} (*T. aestivum* numbers) are separated 2.2 Å and in the right orientation to form a disulfide bond.

of Dundee UK) binds 14-3-3 in a competitive manner respect to GAPN. Docking of this peptide to the 14-3-3ζ crystal structures indicated that it occupies the central binding groove of 14-3-3ζ in an extended conformation (see a model in Fig. 3A). The comparison with crystallographic structures of 14-3-3ζ-peptide complexes [30,37] available in the Protein Databank reveals that a similar amphipathic groove (responsible for the binding of all peptides) is able to accommodate the ARAApSAPA peptide. In all these complexes the phosphate moiety of the pSer performs electrostatic interactions with a positively charged patch established by residues Lys^{49}, Arg^{56} and Arg^{127} (Table 1). This could explain why high-affinity binding of ARAApSAPA to 14-3-3ζ is dependent on phosphorylation. Indeed, binding could not be detected by applying a non-phosphorylated version of this peptide [38]. We conclude that the recognition of the ARAApSAPA peptide involves the canonical 14-3-3 binding groove, with the ability of this peptide to inhibit the binding of GAPN suggesting the enzyme also interacts with residues in the 14-3-3 binding groove.

There is a high degree of conservation between plant and animal 14-3-3 proteins, with a binding site common to all the isoforms [13]. The residues in the dimer interface and the putative ligand-binding surface are invariant among vertebrates, yeast and plants, suggesting a conservation of structure and function throughout the 14-3-3 family [15]. Additionally, little changes were observed in the overall conformation of the bound 14-3-3 molecule when compared to its unbound conformation, with an rmsd of ∼0.4 Å [30]. Considering this information, we used protein coordinates for human 14-3-3ζ to model the complex of plant GAPN–14-3-3.

3.3. Protein–protein docking

Ab initio docking of the complex was calculated on the basis of Protein Database files from 14-3-3ζ (PDB code 1A4O, subunit A and B) and models of plant GAPNs. In addition, to better establish the top model we took into account our recent report demonstrating that the GAPN–14-3-3 complex has a stoichiometry of two 14-3-3 dimers per one GAPN tetramer [9]. Thus, a dimer of 14-3-3ζ was docked to the model of plant GAPN monomer. One thousand putative structures for the complex were obtained from BiGGER [28], a software useful used in the determination of electron transfer complexes [39]. These structures were first evaluated and ranked by an ab initio procedure, which uses an interaction score function. The next step was to use biochemical data filters, in order to rule out incompatible solutions. It has been reported that with some additional information on the residues or regions critical for docking, BiGGER algorithm should provide reasonable models [39]. In order to reduce the number of complexes to a manageable number, and according to available information, the amino acid Ser^{404} from GAPN and Lys^{49}, Arg^{56} and Arg^{127} from 14-3-3 protein were selected and all complexes were sorted by the distances between these amino acids. This procedure was implemented in Chemera program [28].

Fig. 3 shows results of docking between the peptide ARAApSAPA (representing part of the interacting partner, as a guide) or GAPN and 14-3-3. Fig. 3B is a representation of 14-3-3ζ as centre of mass (small sphere). The most favored positions observed are surrounding the Ser^{404} and Ser^{447} residues in GAPN (Fig. 3B), even when Ser^{447} was not included in the biochemical filters. The occurrence of two distinct motifs in a protein involved in the binding of dimeric 14-3-3 may be essential for full interaction [16]. Indeed, amino acids surrounding the Ser^{447} (^{444}QINSAPA) in GAPN are similar to a putative 14-3-3 binding site. This site shows a difference respect to the 14-3-3 canonical binding motif, because it lacks the Arg residue (−3 from pSer). However, such a modification has been reported, as for example in the plant plasma membrane H^+-ATPase, a well-characterized protein interacting with 14-3-3 and also lacking the Arg residue at the −3 position [16]. When 14-3-3ζ backbone was represented (Fig. 3C), the preferred positions are in the central groove, each one is the actual binding domain, for almost all the 14-3-3-target complexes resolved at the present time [13].

Fig. 4 shows the most favored GAPN–14-3-3ζ complex obtained after biochemical filter, with plant GAPN and 14-3-3ζ dimer subunits in ribbon and surface representation, respectively. The interface between 14-3-3ζ and GAPN

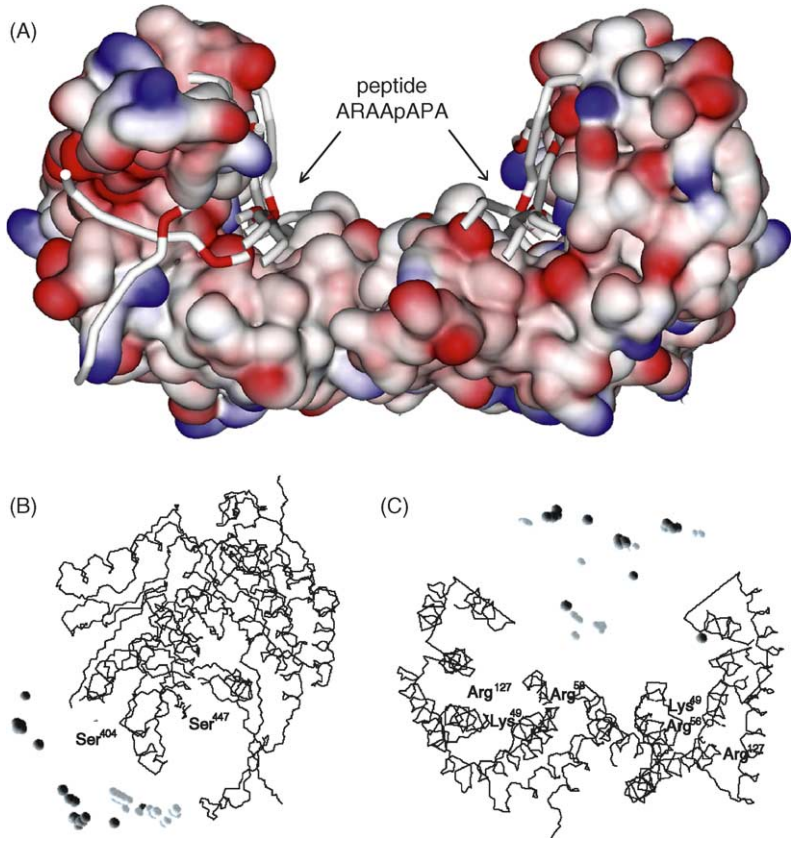

Fig. 3. Docking results of the ARAApSAPA peptide to 14-3-3ζ and GAPN–14-3-3ζ complex. (A) The phosphorylated peptide was docked to GAPN using GRAMM program (see Section 2 for details) the results were mostly docked in the binding groove on 14-3-3. B and C are the 50 best solutions chosen after biochemical data filtering. (B) GAPN is represented as backbone and 14-3-3ζ is represented by its centre of mass using small spheres. (C) Only 14-3-3ζ backbone is represented and small spheres represent the centre of mass of the GAPN.

(Fig. 4A showing side and top down view) exhibits electrostatic (Table 2) and hydrogen bond contacts. The Ser residues 404 and 447 in GAPN are the closest to the side-chain of Lys^{49}, Arg^{56} and Arg^{127} in each monomer of 14-3-3ζ (Fig. 4B). This is in agreement with previous work assigning an interaction between pSer and these residues exclusively [12,13,15,18,34]. In addition, there are seven hydrogen bonds that further stabilize the predicted conformation shown in Fig. 4A. Specifically, the hydrogen bond formed between GAPN NE2 His^{410} and OD2 Asp^{223} in 14-3-3ζ is well conserved [40] (these atoms are at 2.65 Å, with an angle of 18° [25]) (Fig. 4B).

A superimposition of structures (Fig. 4C) shows that the binding motifs of GAPN (^{401}RINSVEE and ^{444}QINSAPA) have an N- to C-terminal orientation opposed to all other available structures. Taking this into consideration, the interaction of the different amino acids could provide very important information to new predictive algorithms. The residues Ile and Asp at −2 and −1 from Ser^{404} respectively, interact with Ile^{217}, Leu^{216} and Leu^{220}, similar to amino

Table 1
Side chain contacts in 14-3-3 complexes

Residue	Mode 1	Mode 2	Non phosphorylated	AANAT	GAPN	
	RSH**S**YPA [30]	RLYH**S**LPA [30]	WL**D**LE [37]	RRH**T**LP [18]	RIN**S**VEE	QIN**S**APA
−4		E180				
−3						Q219
−2	E180 W228	V176 Y179 L227 W228		E180	I217 L216-220	
−1			I166-217, G169, L172-220		I217 L216-220	
0	K49, R56-127 V172	K49, R56-127 V172	K49	K49, R56-127 V172	K49, R56-127	K49, R56-60
+1	I217 L172-216-220	I217 L172-216-220	I166-217, G169, L172-220		S57V61	L227 W228
+2	cis—K49	trans—No intarctions	R56-60	trans—No intarctions	R60	trans—No intarctions

Phosphorylated amino acids, considered as zero position are in bold. Numbers correspond to N to C orientation.

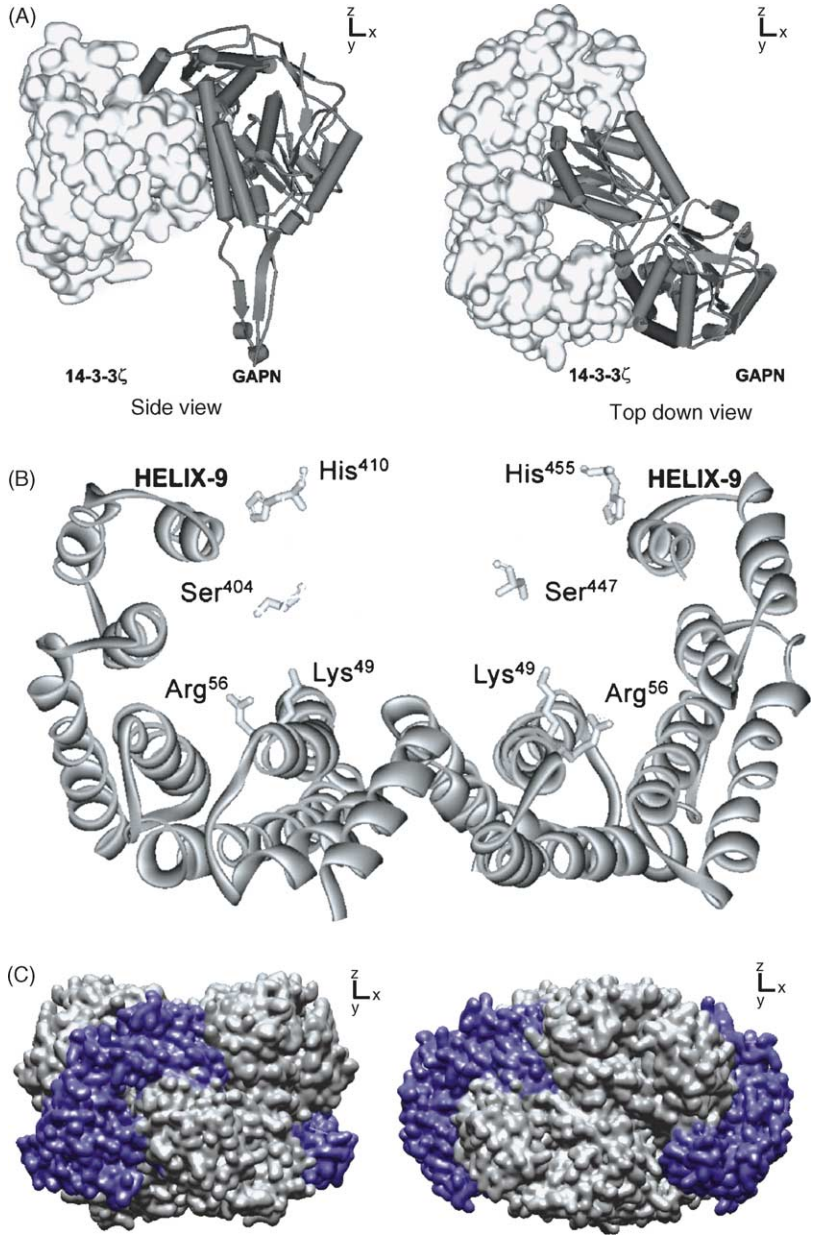

Fig. 4. (A) Side view and top down view of the GAPN–14-3-3ζ complex. Only the interaction between a monomer of the GAPN enzyme and a dimer of 14-3-3 is shown. Ribbon diagram of a GAPN monomer with superimposed spheres that represent the molecular surface of 14-3-3. (B) Ribbon diagram of a 14-3-3ζ dimer showing only the portions of GAPN that interact with 14-3-3ζ. (C) A superimposition of plant GAPN–14-3-3ζ complex on tetramer of GAPN*sm* to obtain a ''native'' complex. 14-3-3ζ are in light blue and GAPN is in grey.

Table 2
Structural complex scores for the interaction between GAPN and 14-3-3

Cross-correlation coefficients	GAPN–14-3-3ζ			
	Site RINSVEE	14-3-3ζ	Site QINSAPA	14-3-3ζ
Area/hydrophobics	−0.5732	0.2950	−0.5715	0.2986
Area/electrostatics	−0.3411	0.4238	−0.3323	0.4316
Hydrophobic complementarity	−0.2889		−0.2869	
Electrostatic complementarity	−0.1506		−0.1520	

All parameters were calculated by Molsurfer [44]. Electrostatic complementarity will result in negative cross-correlation coefficients between the electrostatic-property maps of the two molecules interacting. Positive correlations between hydrophobicities would be indicated by positive hydrophobic complementarity.

acids in position +1 in the mode 1, mode 2 and non phosphorylated WL*D*LE peptides (Table 1). The Val residue +1 from Ser^{404} interacts hydrophobically with Ser^{51} and Val^{61}. The Glu residue at position +2 from Ser^{404}, is at 9.7 Å away from the box-1, and this residue could interact electrostatically with a positively charged patch, specifically with the well-conserved Arg^{60} (Table 1). However, it is possible that alternative conformers, projecting away from the ligands, could bring the side-chain closer to 14-3-3, constituting structural determinants.

An amplified view of the model (showing the interface with Ser^{404} and Ser^{447}) is detailed in Fig. 4B. The phosphate group of the Ser^{404} could be closer than 5 Å from Lys^{49} (Fig. 4B, Table 1). In this conformation, the motif ^{444}QINSAPA (second putative motif in GAPN) contacts the Lys^{49} (9.4 Å, with the phosphate group closer than 6 Å), as well as the residues Arg^{56} and Arg^{127} on the other subunit of 14-3-3ζ dimer (Fig. 4B, Table 1). Distances from the GAPN Ser residues to amino acids in 14-3-3 were calculated to be 7.9 and 9.4 Å to Lys^{49}, 9.4 and 12.4 Å to Arg^{56}, and 10.6 and 12.6 Å to Arg^{127}. These interactions determine the formation of the complex, because the non-phosphorylated form of GAPN does not interact with 14-3-3 [9]. The Gln residue at position −3 from Ser^{447} contacts Gln^{219} in 14-3-3. Similar to amino acid −1 from pSer in mode 2 peptide sequence, Ala +1 interacts with Leu^{227} and Trp^{228} in 14-3-3, which is consistent with opposed orientation of GAPN respect to peptide in mode 2. Pro +2 has trans conformation and no interaction with any other residue was observed. The polypeptide chain of GAPN around Ser^{404} adopts an extended conformation that is most similar to that of the phosphopeptide with the ''non phosphorylated'' consensus sequence (WL*D*LE), although its sequence is closer to the mode 1 sequence. Similarly, the second motif in GAPN has a sequence closer to mode 1, but its interaction with 14-3-3 is most similar to mode 2. This type of phenomenon was also observed in AANAT-14-3-3ζ (see next paragraph), where AANAT has an extended conformation similar to that of the phosphopeptide with the mode 2 consensus sequence, although its sequence is closer to that of the mode 1 [18].

The only case where activation of an enzyme by 14-3-3s is understood at the structural level is serotonin *N*-acetyltransferase (AANAT) [18]. Binding of a 14-3-3 dimer restricts the movement of a floppy loop in AANAT, forcing the enzyme into the conformation that is most favourable for substrate binding [18]. So far, the precise mechanism of regulation by 14-3-3s is still puzzling. AANAT has a canonical binding site, with a Pro residue in position +2 that causes a sharp bend allowing the protein backbone to exit the binding groove of the 14-3-3 protein. On the other hand, while pSer^{483} is clearly involved in the 14-3-3-binding site on PFK-2, the surrounding sequence ^{480}RNYpS^{483}VGS lacks the Pro residue that is typically found in the +2 position of many canonical 14-3-3-binding phosphopeptides [30]. The latter is the case for the first binding motif found in GAPN (^{401}RINSVEE). This site also lacks the Pro residue in +2 position similar to PFK-2 and it is clearly observed that GAPN structure does not sweep away from the binding site sharply (Fig. 4B).

The ability of 14-3-3 to interact via different sets of residues in the groove suggests how 14-3-3 can bind proteins bearing very different sequences. The two-ligand binding grooves in dimeric 14-3-3 are located within the same concave surface, about 30 Å apart. Our results suggest that a ligand bearing a phosphoserine motif could bind in one groove, with another (perhaps unphosphorylated) ligand bound to the second groove [37].

GAPN*sm* exists as a tetramer with four identical subunits related by non-crystallographic 222 symmetry, establishing that the tetramer can be considered as a dimer of dimers [8]. In agreement with this non-equivalent subunits model, it has been reported that in heterotrophic plant cells two kind of GAPN subunit are found: phosphorylated and non-phosphorylated [7]. In order to construct a complete model, we made a superimposition of the predicted structure of GAPN:14-3-3ζ complex with the tetramer of GAPN*sm*, using the program Chemera [28]. Since we have determined a stoichiometry of 1:2 for the complex GAPN (tetramer):14-3-3 (dimer) in plants, we superimposed the monomer of GAPN to subunits A and C of the GAPN*sm* tetramer, as illustrated in Fig. 4C.

3.4. Electrostatic isopotential curves and ionic strength dependence of the GAPN–14-3-3ζ complex

An increase in surface hydrophobicity is produced by the binding of divalent cations to 14-3-3 proteins [19]. Hydrophobic interaction is thus an important force for the formation of 14-3-3-target protein complexes. The importance of these interactions was also revealed by the possibility of purifying stable complexes where the target of 14-3-3 was in a non-phosphorylated state, in the presence of high concentration of salt [41]. However, preferred electrostatic attraction has long been recognized as a driving force to fast complex associations [20,42,43]. Phosphorylated GAPN found in heterotrophic tissues of wheat seems to interact with a 14-3-3 regulatory polypeptide forming a stable complex in the absence of divalent cation [9]. That independence of divalent cation represents a new form of association between a 14-3-3 protein and its specific target. This fact led us to analyse the electrostatic isopotential curves of 14-3-3ζ structure and GAPN models.

We used Molsurfer [44] in order to calculate contact surfaces feature for each protein in the GAPN–14-3-3ζ complex. In this analysis, the relevance in charge complementarity (electrostatic complementarity) between the two canonical binding sites in GAPN and box-1 in 14-3-3ζ suggests that electrostatic forces could be determinant to stabilize the complex (Table 2). Thus, the GAPN electrostatic isopotential curves determine an easily predicted dipolar moment (Fig. 5). Specifically, the environment of two clusters of the 14-3-3ζ binding domains are negatively

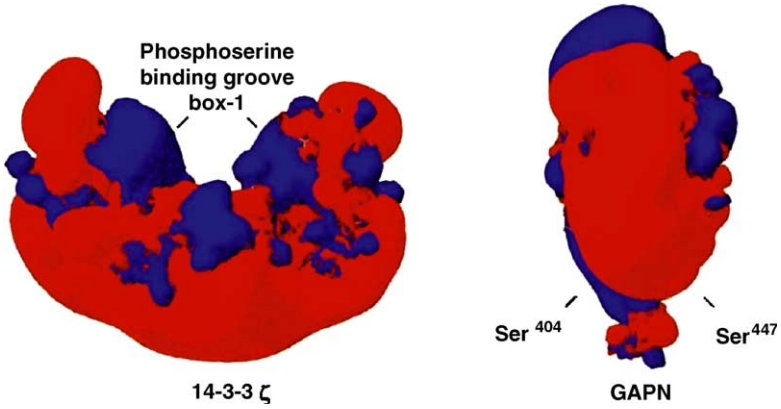

Fig. 5. Isopotential curves of plant 14-3-3ζ (left) and GAPN (right). The positive charges are represented in blue, and negative charges are represented in red. The numbers Ser^{404} and Ser^{447} correspond to *T. aestivum* GAPN.

charged and, in addition, 14-3-3ζ has four zones with different charges (Fig. 5). The box-1 (composed by the three absolutely conserved basic residues in 14-3-3ζ) and its environment form a solitary basic pocket on this otherwise positively charged molecule. Considering the electrostatic properties of the two molecules, one can expect that, if the clusters in GAPN containing Ser^{404} and Ser^{447} are the actual domains interacting with 14-3-3 proteins, the electrostatic attraction could be the driving force for the formation of this complex. The high content of acid residues found around Ser^{404} in GAPN (^{401}RINSVEE, see Fig. 1) should induce a strong dipolar moment. Campbell et al. [45] speculated that the negatively charged Glu residues conferred to the inositol polyphosphate 5-phosphatase the ability to bind 14-3-3ζ in a non-phosphorylated state. These Glu residues at positions +2 and +3 have been demonstrated to be highly conserved in GAPN proteins (Fig. 1). However, the phosphorylated state of GAPN is essential for its binding to 14-3-3 [7,9]. The overall picture suggests that these residues could form ionic bonds with box-1 in 14-3-3 proteins, thus enhancing the electrostatic interactions.

The magnitude of electrostatic attraction in a protein complex can be altered by the addition of monovalent salts to a solution [20,43,46]. The rate of association of GAPN and 14-3-3 has been evaluated in terms of electrostatic interactions. Studies were based on the hysteretic behaviour exhibited by GAPN partially purified from wheat endosperm. This plant tissue contains phosphorylated GAPN forming a complex with 14-3-3 proteins [9]. The reaction catalysed by the GAPN–14-3-3 complex in the presence of exogenous Mg^{2+} (included in the assay medium) shows a remarkable lag phase. However, kinetic curves performed by GAPN–14-3-3 complex or GAPN alone, without divalent cation exhibit no lag phase under the same conditions. This lag phase is thus a consequence of a relatively slow dissociation of the GAPN–14-3-3 complex exerted by the divalent cation. The duration of the lag phase (the time between the initial activity and subsequent steady-state activity) depends on the type and concentration of divalent cation presents in the assay medium. Studying the slow, time-dependent activation of partially purified GAPN induced by Mg^{2+} or Ca^{2+}, it was possible to determine the ionic strength dependence of protein–protein dissociation kinetics. Table 3 shows the effect of ionic strength on the hysteretic behaviour of partially purified GAPN. As shown, at low ionic strength GAPN activity is limited by the rate of dissociation of the protein–protein complex. This dissociation was facilitated as the ionic strength was raised. Because the ionic strength modified the electrostatic interactions, it could be established the importance of electrostatic interactions in the formation of the GAPN–14-3-3 complex. A similar hysteretic behaviour has been previously described for the interaction of nitrate reductase (NR) with 14-3-3 [47]. NR extracted from darkened leaves displays non-linear kinetics. This was proposed to be a consequence of a "tight" binding of a 14-3-3 protein, which is not actually reversed by the removal of Mg^{2+} cation [47]. Recently, this feature was confirmed [26].

3.5. Dependence on pH of the GAPN–14-3-3ζ complex

His is the only amino acid with a pK_a value close to the physiological pH [20,43]. Shifts of pK_as of His residues in proteins afford valuable information about their environ-

Table 3
Hysteretic behaviour in the activity of GAPN

NaCl addition	τ (min)	$V_i \times 10^5$ (U/mg)	$V_{ss} \times 10^3$ (U/mg)
None	2.2	7.9	2.9
+50 mM	1.8	8.0	3.0
+100 mM	1.5	8.2	3.0
+150 mM	1.3	9.1	3.0
+250 mM	1.1	8.9	3.0
+300 mM	1.0	8.6	2.9

Effect of ionic strength on the hysteretic properties exhibited by the GAPN–14-3-3 complex from wheat endosperm. The hysteretic behavior was measured by incubation of the enzyme at the stated concentrations of NaCl prior to assay for activity in the presence of 10 mM $MgCl_2$, as indicated under Section 2. All kinetic parameters are means of at least three determinations and are reproducible within at least ±10%.

Table 4
pH dependence of the occurrence of the GAPN–14-3-3 complex

pH	$V_{ss} \times 10^{-3}$ (U/mg) No Mg^{2+}	$V_{ss} \times 10^{3}$ (U/mg) Plus Mg^{2+}	Activation (folds)
6.5	0.10	0.10	–
7.0	0.20	0.60	3.00
7.7	0.24	0.60	2.50
8.3	0.70	2.60	3.70
8.5	0.80	2.40	3.00
9.0	0.24	0.60	2.50
9.5	0.20	0.20	–

Samples partially purified from wheat endosperm and containing the complex GAPN–14-3-3 were preincubated and assayed for activity at different pH values in the absence or in the presence of 10 mM $MgCl_2$. All kinetic parameters are means of at least three determinations and are reproducible within at least ±10%.

ment [20,43]. We analysed the pH dependence of the GAPN activity as probe of GAPN–14-3-3 complex state (Table 4). It has been previously demonstrated that Mg^{2+} alone has no effect on GAPN activity, but releases the enzyme from its interaction with 14-3-3 [9]. On this basis, we measured activity of partially purified GAPN at different pH values and under two different conditions: with and without 10 mM Mg^{2+}. In this screening, if a certain pH condition exits where there is not interaction between 14-3-3 and GAPN, the activity of the enzyme at such a pH should be the same with or without Mg^{2+}. In agreement with results obtained by Athwal et al. [48] studying the interaction between nitrate reductase and 14-3-3, we observed that at pH 6.8 GAPN activity is not sensitive to Mg^{2+}, owing to a H^+-activation of 14-3-3 proteins. It has been established that plant 14-3-3s can inhibit nitrate reductase in the absence of Mg^{2+} at pH 6.5 (specifically at pH values below 6.8) [48]. This slightly acidic medium has been shown to mimic a pH 7.5 environment in the presence of Mg^{2+}, as far as conformational changes to the protein are concerned. It is likely that the protonation of His residues in 14-3-3 mediates the effect of pH, since its pKa falls within this pH range [48]. The reduced dependence on Mg^{2+} at pH 6.5 reflects the ''H^+-activation'' of the 14-3-3 binding to the targets. The loop 8 region of the 14-3-3 protein has been implicated in mediating Mg^{2+} binding [49], but the basis for H^+-activation is not clear.

Table 4 shows the occurrence of another small change in the action of Mg^{2+} on the activity of partially purified GAPN between pH 7.0 and pH 8.3 (Table 4). There are only two His residues in GAPN, exposed at the interface with 14-3-3, His^{410} and His^{455} (Fig. 4). Theses residues are strictly conserved in plant GAPNs (Fig. 1). It is possible that our results reflect protonation/deprotonation of His^{410}, which forms a hydrogen bond with Asn^{223} (Fig. 4). The His^{455} is near to helix nine in the other subunit of the 14-3-3 dimer (Fig. 4), but we have no information about the correct position of residues situated in this part of 14-3-3ζ, since the structural model was unable to resolve correctly this region of the protein.

4. Conclusions

Our previous reports have shown that in heterotrophic plant cells GAPN is phosphorylated and interacting with a protein of the 14-3-3 family [9]. Based on the crystal structure of 14-3-3ζ, and models of plant GAPNs we propose a detailed description of the structural properties of the complex between both proteins. Our models of the GAPNs binding pocket are mainly predictive, and need to be confirmed experimentally. Thus, in vitro studies site-directed mutagenesis would constitute an important next step towards the validation of our models. This approach constitutes a key tool for the discovery of novel ways for the interaction of 14-3-3 with target proteins.

The model, corresponding to wheat endosperm GAPN–14-3-3ζ complex is presented at different levels of detail. The interacting domain is very similar to the model proposed for other 14-3-3-target protein complexes [18]. In order to explain the dissimilar behaviour of GAPN–14-3-3, where the action of divalent cations (as Mg^{2+} and Ca^{2+}) induces dissociation of the complex [9,19,49], we studied the main force stabilizing the GAPN–14-3-3ζ complex. Electrostatic isopotential curves for GAPN showed that this protein has two zones, one with a net positive charge and another neatly negative. The hydrophobicity change in the surface of 14-3-3ζ by the union of divalent cation could destabilize the GAPN–14-3-3 complex, which constitutes an opposite behaviour in respect to that found for the interaction of 14-3-3 with other proteins. In agreement with this, the alteration of ionic strength in the medium altered the slow, time-dependent activation of GAPN induced by Mg^{2+}. Thus, we present a hypothetical model that best fits current theoretical and experimental information and that explains the odd behaviour of the GAPN–14-3-3 complex respect to the effect of divalent cations. Further experimental work would be necessary to determine the complete validity of the model.

Acknowledgments

This work was supported in part by grant PICT'03 1-14733 from Agencia Nacional de Promoción Científica y Tecnológica (ANPCyT, Argentina). DMB is a Fellow and AAI a Investigator Career Member from Consejo Nacional de Investigaciones Científicas y Técnicas (CONICET, Argentina).

References

[1] A. Habenicht, The non-phosphorylating glyceraldehyde-3-phosphate dehydrogenase: biochemistry, structure, ocurrence and evolution, Biol. Chem. 378 (1997) 1413–1419.
[2] S. Marchal, D. Cobessi, S. Rahuel-Clermont, F. Tete-Favier, A. Aubry, G. Branlant, Chemical mechamism and substrate binding sites of NADP-dependent aldehyde dehydrogenase from Streptococcus mutans, Chem. Biol. Interact. 130 (2001) 15–28.

[3] A.A. Iglesias, On the metabolism of triose-phosphate in photosynthetic cells. Their involvement on the traffic of ATP and NADPH, Biochem. Edu. 18 (1990) 2–5.
[4] M. Mateo, A. Serrano, Occurrence of phosphorylating and non-phosphorylating NADP-dependent glyceraldehyde-3-phosphate dehydrogenase in photosynthetic organisms, Plant Sci. 84 (1992) 163–170.
[5] D.A. Boyd, D.G. Cvitkovitch, I.R. Hamilton, Sequence, expression, and function of the gene for the non-phosphorylating, NADP-dependent glyceraldehyde-3-phosphate dehydrogenase of *Streptococcus mutants*, J. Bacteriol. 177 (1995) 2622–2627.
[6] G.J. Kelly, M. Gibbs, Nonreversible D-glyceraldehyde-3-phosphate dehydrogenase of plant tissue, Plant Physiol. 52 (1973) 111–118.
[7] D.M. Bustos, A.A. Iglesias, Non-phosphorylating glyceraldehyde-3-phosphate dehydrogenase is post- translationally phosphorylated in heterotrophic cells of wheat (*Triticum aestivum*), FEBS Lett. 530 (2002) 169–173.
[8] D. Cobessi, F. Tête-Favier, S. Marchal, G. Branlant, A. Aubry, Apo and holo crystal structure of an NADP-dependent aldehyde dehydrogenase from *Streptococcus mutants*, J. Mol. Biol. 290 (1999) 161–173.
[9] D.M. Bustos, A.A. Iglesias, Phosphorylated non-phosphorylating glyceraldehyde-3-phosphate dehydrogenase from heterotrophic cells of wheat interacts with 14-3-3 proteins, Plant Physiol. 133 (2003) 2081–2088.
[10] A.U. Igamberdiev, L.E. Kleczkowski, Implications of adenylate kinase-governed equilibrium of adenylates on contents of free magnesium in plant cells and compartments, Biochem. J. 360 (2001) 225–231.
[11] W.C. Plaxton, The organization and regulation of plant glycolysis, Annu. Rev. Plant Physiol. Plant Mol. Biol. 47 (1996) 185–214.
[12] P. Sehnke, J. Delille, R. Ferl, Consummating signal transduction: the role of 14-3-3 proteins in the completion of signal-induced transitions in protein activity, Plant Cell (2002) S339–S354.
[13] S. Comparot, G. Lingiah, T. Martin, Function and specificity of 14-3-3 proteins in the regulation of carbohydrate and nitrogen metabolism, J. Exp. Botany 54 (2003) 595–604.
[14] B. Xiao, S.J. Smerdon, D.H. Jones, G.G. Dodson, Y. Soneji, A. Aitken, S.J. Gamblin, Structure of a 14-3-3 protein and implications for coordination of multiple signalling pathways, Nature 376 (1995) 188–191.
[15] D. Liu, J. Bienkowska, C. Petosa, R.J. Collier, H. Fu, R. Liddington, Crystal structure of the zeta isoform of the 14-3-3 protein, Nature 376 (1995) 191–194.
[16] A. Aitken, H. Baxter, T. Dubois, S. Clokie, S. Mackie, K. Mitchell, A. Peden, E. Zemlickova, 14-3-3 proteins in cell regulation. Specificity of 14-3-3 isoform dimer interactions and phosphorylation, Biochem. Soc. Trans. 30 (2002) 351–360.
[17] A.J. Muslin, H. Xing, 14-3-3 proteins: regulation of subcellular localization by molecular interference, Cell Signal 12 (2000) 703–709.
[18] T. Obsil, R. Ghirlando, D. Klein, S. Ganguly, F. Dyda, Crystal structure of the 14-3-3ζ:serotinin *N*-acetyltransferase complex: a role for scaffolding in enzyme regulation, Cell 105 (2001) 257–267.
[19] G.S. Athwal, J.L. Huber, S.C. Huber, Biological significance of divalent cation binding to 14-3-3 proteins in relationship to nitrate reductase inactivation, Plant Cell Physiol. 39 (1998) 1065–1072.
[20] G. Schreiber, Kinetics studies of protein–protein interactions, Curr. Opin. Struct. Biol. 12 (2002) 41–47.
[21] W.N. Kaiser, S.C. Huber, Post-translatinal regulation of nitrate reductase: mechanisms, physiological relevance and environmental triggers, J. Exp. Botany 52 (2001) 1981–1989.
[22] M. Pozuelo Rubio, K.M. Geraghty, B.H. Wong, N.T. Wood, D.G. Campbell, N. Morrice, C. Mackintosh, 14-3-3-affinity purification of over 200 human phosphoproteins reveals new links to regulation of cellular metabolism, proliferation, and trafficking, Biochem. J. 1 (2004) 1–2.
[23] B. Morgenstern, A. Dress, T. Werner, Multiple DNA and protein sequence alignment based on segment-to-segment comparison, Proc. Natl. Acad. Sci. U.S.A. 93 (1996) 12098–12103.
[24] A. Sali, T.L. Blundell, Comparative protein modelling by satisfaction of spatial restraints, J. Mol. Biol. 234 (1993) 779–815.
[25] R. Rodriguez, G. Chinea, N. Lopez, T. Pons, G. Vriend, Homology modeling, model and software evaluation: three related resources, CABIOS 14 (1998) 523–528.
[26] W. Shen, C. Clark, S.C. Huber, The C-terminal tail of *Arabidopsis* 14-3-3ω functions as an autoinhibitor and may contain a tenth α-helix, Plant J. 34 (2003) 473–484.
[27] S.J. Weiner, P.A. Kollman, D.A. Case, U.C. Singh, C. Ghio, G. Alagona, S. Profeta, P. Weiner, A new force field for molecular mechanical simulation of nucleic acids and proteins, J. Am. Chem. Soc. 106 (1984) 765–784.
[28] P.N. Palma, L. Krippahl, J.E. Wampler, J.J.G. Moura, BiGGER: a new (Soft) docking algorithm for predicting protein interactions, PROTEINS: Struct. Funct. Genet. 39 (2000) 372–384.
[29] E. Katchalski-Katzir, I. Shariv, M. Eisenstein, A.A. Friesem, C. Aflalo, I.A. Vakser, Molecular surface recognition: determination of geometric fit between proteins and their ligands by correlation techniques, Proc. Natl. Acad. Sci. U.S.A. 89 (1992) 2195–2199.
[30] K. Rittinger, J. Budman, J. Xu, S. Volinia, L.C. Cantley, S.J. Smerdon, S.J. Gamblin, M.B. Yaffe, Structural analysis of 14-3-3 phosphopeptide complexes identifies a dual role for the nuclear export signal of 14-3-3 in ligand binding, Molec. Cell 4 (1999) 153–166.
[31] D.F. Gómez Casati, J.I. Sesma, A.A. Iglesias, Structural and kinetic characterization of NADP-dependent, non-phosphorylating glyceraldehyde-3-phosphate dehydrogenase from celery leaves, Plant Sci. 154 (2000) 107–115.
[32] K.E. Neet, G.R.J. Ainslie, Hysteretic enzymes, in: D.L. Purich (Ed.), Methods in Enzymology, vol. 64, Academic Press, New York, 1980, pp. 192–226.
[33] S.P.J. Brooks, A simple computer program with statistical tests for the analysis of enzyme kinetics, Biotechniques 13 (1992) 906–911.
[34] G. Tzivion, J. Avruch, 14-3-3 proteins: active cofactors in cellular regulation by serine/threonine, J. Biol. Chem. 277 (2002) 3061–3064.
[35] M. Pozuelo Rubio, M. Peggie, B.H.C. Wong, N. Morrice, C. Mackintosh, 14-3-3s Regulate fructose-2,6-bisphosphate levels by binding to PKB-phosphorylated cardiac fructose-2,6-bisphosphate kinase/phosphatase, EMBO J. 22 (2003) 3514–3523.
[36] I. O'kelly, M.M. Butler, N. Zilberberg, S.A.N. Goldstein, Foward transport: 14-3-3 binding overcomes retention in endosplasmic reticulum by dibasic signals, Cell 11 (2002) 577–588.
[37] C. Petosa, S.C. Masters, L.A. Bankston, J. Pohli, B. Wang, H. Fu, R.C. Liddington, 14-3-3ζ Binds a phosphorylated raf peptide and an unphosphorylated peptide via its conserved amphipathic groove, J. Biol. Chem. 273 (1998) 16305–16310.
[38] F.C. Milne, G. Moorhead, M. Pozuelo Rubio, B. Wong, A. Kulma, J.E. Harthill, D. Villadsen, V. Cotelle, C. Mackintosh, Affinity purification of diverse plant and human 14-3-3-binding partners, Biochem. Soc. Trans. 30 (2002) 379–381.
[39] L. Krippahl, J.J.G. Moura, P.N. Palma, Modeling protein complexes with BiGGER, PROTEINS: Struct. Funct. Genet. 52 (2003) 19–23.
[40] M. Würtele, C. Jelich-Ottmann, A. Wittinghofer, C. Oecking, Structural view of a fungal toxin acting on a 14-3-3 regulatory complex, EMBO J. 22 (2003) 987–994.
[41] M.C. Morris, A. Heitz, J. Mery, F. Heitz, G. Divita, An essential phosphorylation-site domain of human cdc25C interacts with both 14-3-3 and cyclins, J. Biol. Chem. 37 (2000) 28849–28857.
[42] I. Halperin, B. Ma, H. Wolfson, R. Nussinov, Principles of docking: an overview of search algorithms and a guide to scoring functions, PROTEINS: Struct. Funct. Genet. 47 (2002) 409–443.
[43] T. Selzer, G. Schreiber, New insights into the mechanism of protein–protein association, PROTEINS: Struct. Funct. Genet. 45 (2001) 190–198.

[44] R.R. Gaddoulline, R.C. Wade, D. Walther, MolSurfer: two dimensional maps for navigating three-dimensional structures of proteins, Trends Biochem. Sci. 24 (1999) 285–287.
[45] J.K. Campbell, R. Gurung, S. Romero, C.J. Speed, R.K. Andrews, M.C. Berndt, C.A. Mitchell, Activation of the 43 kDa inositol polyphosphate 5-phosphatase by 14-3-3ζ, Biochemistry 36 (1997) 15363–15370.
[46] S.R. Kimura, R.C. Brower, S. Vajda, C. Camacho, Dynamical view of the positions of key side chains in protein–protein recognition, Biophys. J. 80 (2001) 635–642.
[47] S.C. Huber, J.L. Huber, Metabolic activator of spinach leaf nitrate reductase: effect on enzymatic activity and desphosphorylation by endogenous phosphatase, Planta 196 (1995) 180–189.
[48] G.S. Athwal, C.R. Lombardo, J.L. Huber, S.C. Masters, H. Fu, S.C. Huber, Modulation of 14-3-3 protein interactions with target polypeptides by physical and metabolic effectors, Plant Cell Physiol. 41 (2000) 523–533.
[49] G.S. Athwal, S.C. Huber, Divalent cations and polyamines bind to loop 8 of 14-3-3 proteins, modulating their interaction with phosphorylated nitrate reductase, Plant J. 29 (2002) 119–129.